



An enhancement to sea ice motion and age products

Mark A. Tschudi¹, Walter N. Meier², J. Scott Stewart²

¹CCAR, Department of Aerospace Engineering Sciences, University of Colorado-Boulder, UCB 431, Boulder, CO, USA, 80309

5 ²National Snow and Ice Data Center, CIRES, University of Colorado-Boulder, UCB 449, Boulder, CO, USA, 80309

Correspondence to: Mark A. Tschudi (mark.tschudi@colorado.edu)

Abstract. A new version of the sea ice motion and age products distributed at the National Snow and Ice Data Center's NASA Snow and Ice Distributed Active Archive Center has been developed. The new version, 4.0, includes several significant upgrades in processing, corrects known issues with the previous version, and updates the time series through 2018, with regular updates planned for the future. Here, we provide a history of the product development, discuss the improvements to the algorithms that create these products, and compare the Version 4 products to the previous version. While Version 4 algorithm changes were significant, the impact on the products is relatively minor, particularly for more recent years. Trends in motion and age are not substantially different between the versions. Changes in sea ice motion and age derived from the product show a significant shift in the Arctic ice cover, from a pack with a high concentration of older ice, to a sea ice cover dominated by first-year ice, which is more susceptible to summer melt. We also observe an increase in the speed of the ice in recent years, which is anticipated with the annual decrease in sea ice extent.

1 Introduction

Arctic sea ice conditions have undergone significant changes in recent years with dramatic reductions in the overall ice extent, ice age, and ice thickness. The decline in Arctic sea ice extent is one of the better-known and more striking examples of a changing Arctic [e.g. Meier *et al.*, 2014; Comiso *et al.*, 2008; 2012; 2017a; Stroeve *et al.*, 2011; 2012; 2014a]. Recent estimates indicate that September Arctic sea ice extent has decreased by approximately 13% per decade since 1979, with record or near-record minimum extents occurring several times in the last few years [e.g., Perovich *et al.*, 2018]. In the Antarctic, the trends are smaller and there is higher interannual variability [e.g., Parkinson and Cavalieri, 2012]; overall the Antarctic trends are slightly positive, but with strong regional variability [Comiso *et al.*, 2017b].

25 Data on sea ice thickness are far less comprehensive and it is more difficult to draw solid quantitative thickness or volume trends. However, there is broad evidence, from observations [e.g., Kwok, 2018] and models [e.g., Stroeve *et al.*, 2014] that Arctic sea ice thinning trends are even stronger than the extent decrease. One explanation for the stronger decline in ice thickness is the preferential loss of thicker, old ice in comparison with relatively thin first-year ice. For example, Johannessen *et al.* [1999] and Comiso *et al.* [2008, 2012] noted the decline in multiyear sea-ice was roughly twice that of first-year ice. In



a study examining ice age since the early 1980s, *Maslanik et al.* [2011] found continued recent loss of the oldest ice types, which accelerated starting in 2005. This trend has continued through 2018 [*Perovich et al.*, 2018; *Kwok*, 2018].

5 A continued decline in the sea-ice cover and the shift from thick multiyear ice (MYI) to more easily navigable first-year ice (FYI) arguably will have one of the biggest impacts on humans and the Arctic environment [e.g., *Pizzolato et al.*, 2016]. In particular, the prospect of new shipping lanes, extraction of oil and gas from previously inaccessible regions, and increased national security concerns associated with easier and more accessible Arctic waters have already been identified as significant economic and cultural changes related to the sea-ice cover [*Huntington et al.*, 2007]. More open water along the coast will also add to the risk of storm surge and coastal erosion [*Vermaire et al.*, 2013; *Francis et al.*, 2006, 2005; *Lynch et al.*, 2004] and
10 there is some evidence that reductions in sea ice may affect locations far from the Arctic [e.g., *Overland et al.*, 2016], manifesting particularly through extreme weather in the mid-latitudes [e.g., *Cohen et al.*, 2014; *Francis and Vavrus*, 2012].

The distribution of the age of Arctic sea ice contributes to the vulnerability of the ice cover during the melt season because older ice is on average thicker than younger ice [*Tschudi et al.*, 2016a]. Younger ice is more susceptible to deformation and
15 melts out more readily during the summer, whereas older ice is more likely to remain through the melt season if it does not advect out of the Arctic Ocean. The pre-melt fractional distribution of ice age may therefore serve as a descriptive predictor of how much sea ice will disappear during the melt season and indicate where summer ice loss is more likely to occur.

Ice thickness observations are becoming more widely and readily available from satellite altimeters such as NASA's Ice, Cloud, and land Elevation Satellite (ICESat) [*Kwok and Cunningham*, 2008] and ESA's CryoSat-2 [*Laxon et al.*, 2013; *Kurtz et al.*, 2014]. However, these satellite-derived data cover a limited time span. ICESat collected twice-yearly monthly estimates from 2003 to 2008 and CryoSat-2, launched in 2010, produces complete Arctic-wide fields monthly [*Tilling et al.*, 2016]. Satellite-derived observations will expand greatly with the launch of the NASA ICESat-2 in September 2018 [*Markus et al.*, 2017]. Submarine upward-looking sonar has also been used to estimate thickness sporadically since the 1950s over a selected
25 region in the central Arctic. These data have been connected to the satellite altimetry record [*Kwok*, 2018] to create an intermittent long-term timeseries over part of the Arctic. While these direct ice thickness estimates are useful, such products lack the long-term and/or the basin-wide coverage that is available from the multi-decadal sea ice age record.

In contrast, sea ice motions derived from satellite instruments and buoys [*Tschudi et al.*, 2016b] can be used to obtain a
30 continuous, complete, long-term record of sea ice ice age [*Tschudi et al.*, 2019c]. Because of its length and completeness, this ice age timeseries has been used in several studies [*Maslanik et al.*, 2007, 2011; *Tschudi et al.*, 2010] and reviews of Arctic change [*Stroeve et al.*, 2011; *Meier et al.*, 2014; *Perovich et al.*, 2016] to assess changes in the ice cover. Over time, enhancements and improvements have been made to the ice motion and ice age products. The latest version of the ice age product addresses issues noted by users [*Szanyi et al.*, 2016] and both products are enhanced through a refined optimal



interpolation approach that improves the spatial continuity of the gridded motion and age fields. Our focus in this paper is to highlight the changes in the new version, compare the new version with older versions, and provide an updated assessment of ice age trends. As further background, we also document the algorithms and production of the Polar Pathfinder Daily 25 km EASE-Grid Sea Ice Motion Vectors product [Tschudi et al., 2016b] and the EASE-grid Sea Ice Age product [Tschudi et al., 5 2016c]. The age product is produced by utilizing the sea ice motion product. We therefore outline the production of the motion product first.

2 The Polar Pathfinder Sea Ice Motion Product

The “Polar Pathfinder 25 km EASE-Grid Sea Ice Motion Vectors” product [Tschudi et al., 2016b] is archived and distributed by the NASA Snow and Ice Distributed Active Archive Center (DAAC) at the National Snow and Ice Data Center (NSIDC). 10 The sea ice motion product provides gridded daily estimates and weekly and monthly averages of ice motions for both the Arctic and Antarctic regions. This is a popular product for the research community having over 3400 unique users since its introduction in 2011 [NSIDC, personal comm.]. In this section, we describe the basic processing methodology and data sources along as well as noting the changes made in the new Version 4 of the product. The version history of the motion product (and the age product discussed in Section 3) is summarized in Table 1, including the release date and enhancements for each version. 15

2.1 Sea ice motion data sources and derivation techniques

There are three primary types of sources for ice motion: (1) gridded satellite imagery – from several sources, (2) winds from reanalysis fields, and (3) buoy position data. Motions are independently derived from each of the sources. A complete daily gridded product is then produced by combining all sources via an optimal interpolation scheme (Figure 1). 20

Gridded satellite imagery

The approach used for deriving ice motion from satellite imagery is a feature-tracking method that uses cross correlations between features in coincident images separated by a given time interval. Specifically, for our product, motion vectors are 25 computed using a maximum cross-correlation (MCC) feature-matching method [Emery et al., 1991, 1995]. Two geolocated, spatially-coincident, temporally-consecutive satellite images are selected. For each valid sea ice grid cell, a “search window” is defined for a region around that grid cell. The later image is translated relative to the earlier image within this search window, and the correlation between the two images is calculated for each translation. The highest correlation value, i.e., the correlation peak, is determined to be the offset in the position of the grid cell between the earlier and the later image; then, the ice velocity 30 is computed by dividing this offset by the time separation between images.



The imagery sources have changed over time, depending on which inputs have been available. The primary source has been passive microwave imagery from a series of sensors. Horizontal and vertical polarization fields of 37 GHz and 85 GHz channels are used when available. These began in late 1978 with the Scanning Multichannel Microwave Radiometer (SMMR) on the NASA Nimbus-7 platform. This operated until August 1987. After SMMR, a series of Special Sensor Microwave
5 Imagers (SSM/I) on U.S. Defense Meteorological Satellite Program (DMSP) platforms carried on the time series. These were used for the motion product through 2006. Starting in 2007, the motion product transition to the DMSP successor instrument, the Special Sensor Microwave Imager and Sounder (SSMIS), of which three still continue to operate (as of February 2019). The SSM/I and SSMIS imagery are from the DMSP SSM/I-SSMIS Daily Polar Gridded Brightness Temperatures, Version 4 product [Maslanik and Stroeve, 2004] and the SMMR imagery are from the Nimbus-7 SMMR Polar Gridded Radiances and
10 Sea Ice Concentrations, Version 1 product [Gloersen, 2006].

These SMMR-SSM/I-SSMIS sources are useful because they provide complete daily coverage in all-sky conditions (i.e., including night and through clouds). However, their low spatial resolution (25 km gridded) limits the resolution of motion estimates that can be retrieved. For example, for the SSM/I-SSMIS fields, with a gridded a resolution of 25 km, daily velocity
15 can only be estimated to the nearest 25 km/day for each velocity component. For this reason, many similar motion product use image pairs separated by more than one day. However, our product obtains useful daily motions by applying an oversampling procedure – effectively moving the correlation window fractions of grid cells – to obtain sub-pixel resolution. An oversampling of 4X has been found to be most effective and is applied to all satellite estimates. This improves the SSM/I-SSMIS effective sampling interval to 6.25 km/day, which corresponds to a motion precision of 7.23 cm/s.

20 In 2002, a more advanced passive microwave sensor, the NASA/JAXA Advanced Microwave Scanning Radiometer for the Earth Observing System (AMSR-E), was launched on the NASA Aqua satellite and operated until October 2011. AMSR-E has more than double the spatial resolution of the previous sensor, 6.25 km gridded resolution for some channels, so its motion resolution is likewise improved. So, during this period (2002-2011), it was also used as source for ice motions. In 2012, JAXA
25 launched AMSR2 on their Global Change Observation Mission – Water (GCOM-W) satellite, which continues to operate (as of February 2019). AMSR2 has not yet been added as a source, but this is planned for a future release of the motion product.

For the period, 1981-2000, vectors were produced from the Advanced Very High Resolution Radiometer (AVHRR). AVHRR is a visible/infrared sensor that provides higher spatial resolution than the passive microwave sources. Daily gridded
30 composites at 4 km resolution were used as input to the maximum cross-correlation algorithm. The higher resolution of the sensor provides more accurate motion estimates than the SMMR-SSM/I record. However, motions can only be derived when there are cloud-free conditions on consecutive days. This yields relatively few vectors, and the impact of AVHRR is relatively small. With the advent of AMSR-E, having similar spatial resolution (6.25 km vs. 4 km) as AVHRR, but with the advantage of all-sky capability resulting in far more motion estimates, AVHRR was discontinued after 2000.



To further reduce errors, post-processing filtering techniques are applied to the cross-correlation scheme. First, a minimum correlation threshold of 0.4 is applied. This removes ‘weak’ matches that are more likely to be incorrect. Second, a neighborhood filter is applied. At the low-resolution of the satellite data, motion is spatially well-correlated across several grid cells. Retrieved vectors that do not agree significantly with at least two neighboring estimates are considered to likely be in error and are rejected. These erroneous vectors occur frequently near the ice edge.

Version 4 changes. There have been two significant changes made to the satellite imagery processing for Version 4. First, the final quality-controlled and calibrated passive microwave brightness temperatures [Maslanik and Stroeve, 2004] have been used throughout the record. In previous versions, near-real-time brightness temperatures [Maslanik and Stroeve, 1999] were used to augment the time series and there was not good provenance on when the near-real-time or final source was used. Another change corrected over-filtering of passive microwave vectors that removed valid motion estimates in Version 3 of the product. This had a relatively small effect in the Arctic because the multiple motion sources provided nearby motion estimates to compensate for the lack of microwave estimates; however, in the Antarctic, where the passive microwave estimates provide the only motion information, the sparser motion estimates often resulted in unrealistic circulation patterns.

Reanalysis winds

The satellite imagery sources are augmented in the Arctic with motions derived from wind forcing using the NCEP/NCAR Reanalysis [Kalnay et al., 2016]. Wind-derived motions are not currently used in the Antarctic. The ice motions estimates are derived based on a simple relationship between winds and ice motion. The sea ice is assumed to move in the geostrophic wind direction, as provided by the reanalysis fields, with a magnitude of 1% of the wind speed, which is similar to the recommendations of Thorndike and Colony [1982]. No changes were made to the wind-derived motions for Version 4. In a future version, we plan to revisit this relationship in the Arctic and investigate adding wind-driven motions for the Antarctic.

Buoy positions

Ice motion vectors are also computed by incorporating position data from the network of drifting buoys deployed as part of the International Arctic Buoy Program [IABP, 2008]. These buoys monitor meteorological and oceanographic data for real-time operational requirements and research purposes, and provide ice motion by transmitting updated locations. This product uses the twice daily (midnight and noon) locations of the IABP "C" buoy product. Two motion estimates are computed from these locations: one from noon of one day to noon of the following day, and one from midnight of a day to midnight the following day.



Version 4 changes. The principal change for the buoys is how the twice-daily observations are integrated into a daily product. Previous versions of this product considered these motions independently of each other and effectively used the most recent observation for a day. In Version 4 the two estimates are averaged to provide one daily motion estimate for each buoy. Also, the IABP source product recently started including floatable buoys, resulting in motion estimates from off the ice. These were not screened out in earlier versions. The effect was relatively small and primarily influenced motions near the ice-edge because of the distance-weighting interpolation. Version 4 now applies an ice mask to the buoys, making the buoy motion domain consistent with the other sources.

Masks for valid motions

Two masks are applied to limit motion retrievals to only regions where sea ice exists. First, a modified land mask is applied. The standard land mask is "dilated" so that cells near land are also excluded because motion retrievals near the coast are unreliable due to the effects of mixed land and ice/ocean grid cells. Because of its narrow channels, the Canadian Archipelago region is also masked out.

Second, a sea ice mask is also applied to limit motion retrievals to only ocean regions that are ice-covered on the days under consideration. The mask is based on the "Sea Ice Concentrations from Nimbus-7 SMMR and DMSP SSM/I-SSMIS Passive Microwave Data, Version 1" at NSIDC [Cavalieri *et al.*, 1996]. The mask defines all areas with concentrations greater than 15% as ice-covered so that valid ice motions can be computed.

Version 4 changes. Previously, the sea ice mask from only the first day was used to define the valid motion region. This was changed in Version 4 to allow motions only where ice is present on both days used to retrieve motions. This results in very small changes near the ice edge. As noted above, the mask is now applied to buoys as well as the other sources.

2.2 Uncertainty of motion estimates

Errors in the ice motion and ice age products are dependent on the resolution of the satellite sensor, as well as geolocation and binning errors for each image pixel [Meier, 2009]. The distance precision of motion detection is limited by the grid cell resolution – a feature can nominally be "observed" to move only an integer number of grid cells. Particularly for the low-resolution inputs, this yields high uncertainty for each individual estimate and an overall noisy motion field.

As noted above, for a 25 km gridded input with 4X oversampling, the limit of precision of the motion is 7.23 cm/s. Atmospheric effects and temporal variability of the surface are additional sources error, especially in the summer. However, several evaluation studies have found that in practice errors are often lower because the different sources of error offset each other.



Kwok et al. [1998] compared ice motion estimated from the European Space Agency (ESA) Remote Sensing Satellite (ERS-1) synthetic aperture radar (SAR) along with drifting buoy motion to the Lagrangian motion product and found an error of 5-12 km/day (~6-14 cm/s). *Meier et al.* [2000], comparing with buoys, found RMS errors of SSMI-derived daily velocity components to vary between ~5-7 cm/s, depending on conditions, with near-zero bias. AMSR-E, with higher spatial resolution, has velocity component errors of 4-5 cm/s [*Meier and Dai*, 2006; *Kwok*, 2008]. *Sumata et al.* [2014] found a correlation coefficient of 0.94 and 0.87 when comparing the ice motion data to IABP buoy drift in winter and summer, respectively. Summertime drift error was higher due in part to surface melt, which affects the passive microwave identification of ice parcels. The largest drift error is found in the fall, which is likely due to formation of new ice [*Meier et al.*, 2000]. Optimal interpolation (discussed below) reduces errors through its error and distance-based weighting, particularly when buoys are incorporated. Temporal averaging further reduces errors in the weekly estimates.

In addition, the errors are not generally cumulative. This is because the motions are largely unbiased, which means that errors in long-term (weeks to months) displacement are relatively small. *Tschudi et al.* [2009] compared drift tracks composed from the sea ice motion product to the drift of the Surface Heat Budget of the Arctic Ocean (SHEBA) ice camp [*Uttal et al.*, 2002] and found a drift error of 27 km over 293 days. Ice motion estimates in the Antarctic are not easily validated due to the lack of buoys for comparison. Generally, Antarctic motions are considered to be less accurate due to the lack of buoys, the more dynamic nature of the Antarctic sea ice, and the larger variability in microwave emission (e.g., flooding and snow-ice formation), limiting the effectiveness of the cross-correlation scheme.

2.3 Combined gridded sea ice motion fields

Daily motion fields are provided from each of the sources during their period of availability. However, for many users, the most useful parameter is the combined gridded product. This combines via an optimal interpolation scheme all available sources for a given day onto a version of the 25 km EASE-Grid [*Brodzik et al.*, 2002]. For further information and the grid, see NSIDC's documentation for this data product [*Tschudi et al.*, 2016b]. For each 25-km ice EASE-grid cell, the speeds (cm/s) in the EASE-grid x-direction (u velocity component) and y-direction (v velocity component) are stored. The daily motions fields are also averaged into weekly and monthly fields.

Optimal interpolation is not simply a spatial average, but also takes into account the accuracy of different sources and the spatial distribution of the source estimates. The motion estimates vary in expected quality with buoys considered most accurate, followed by passive-microwave and/or AVHRR-based estimates and finally by the wind field. This weighting is of the form:

$$w = C e^{(-d/D)} \quad (1)$$



where w is the weight, C is a source-based coefficient (0.45 for wind, 0.95 for buoy, 0.8 for other sources), d is the Euclidean distance between the pixel in question and the motion estimate on the EASE grid, and D is the length-scale over which the estimates are correlated. Thus, estimates that are closer (low d) and higher quality (sources with high C , e.g. buoys), are weighted higher. We assume that buoys are by far the most accurate motion source and are assigned a high C value of 0.95.

5 We use the buoys as the baseline for estimating the other weights. The values of C for the other sources were estimated *a priori* based on comparisons between the source motions and buoy estimates. The correlation length-scale, D , was also estimated empirically, based on cross-correlations of estimates separated by varying distances. The method loops through all grid cells in the domain that are flagged as sea ice-covered. Figure 2 shows an example of the individual motion sources and the resulting combined motion field. The optimal interpolation converts the sparse and/or noisy individual motion fields into a complete

10 and smoothly varying combined motion grid.

Version 4 changes. The most notable change in the motion product for Version 4 involves the optimal interpolation approach. In previous versions, the combined estimate at each valid grid cell was estimated by interpolating the surrounding 15 closest vectors. While this generally gives a good spatial distribution around grid cells, it does not necessarily include all estimates

15 that fall within correlation length-scale and that theoretically could influence interpolated estimate. This means that discontinuities can potentially occur, particularly as highly-weighted estimates (i.e., buoys) fall off the list of closest estimates. When the buoy motion estimates differ significantly from other sources, artificially large spatial gradients in velocity magnitude can arise [Szyani *et al.*, 2016]. In Version 4 of the product, the methodology has been revised to use the 15 highest-weighted ice motion vectors at each grid cell, regardless of source. This means that higher weighted observations have

20 influence over a longer distance and their influence drops off more gradually. This approach significantly reduces and often removes the discontinuity artifact in the daily interpolated product (Figure 3).

As noted above, the Version 4 algorithm also eliminates an over-filtering of SSMI, SSMIS, and AMSR-E passive microwave vectors that occurred in Version 3. Since these vectors are the only source in the Antarctic, they are the only input to the

25 optimal interpolation. The over-filtering of the vectors resulted in the interpolated motion field of the Antarctic ice motion field often being driven by very few underlying motion estimates. This led to unrealistic circulation patterns in the Antarctic because there were too few vectors to create a representative field. The effect also occurred in the Arctic but was much more limited because other sources exist to augment the passive microwave estimates. Version 4 corrects this over-filtering, yielding more passive microwave motion estimates over a broader area, particularly in the Antarctic. An example of this is shown in

30 Figure 4 where the Version 3 product has very few vectors. In the eastern Weddell Sea, this results in southward onshore ice motion. This would be very unusual for the region and comparisons with winds (not shown) show that this motion is not realistic. Version 4 yields more source vectors that better represents the spatial variation in the region. The result is a general eastward circulation, which is more typical for the region and agrees with the wind field.



A final change in the motion product for Version 4 is that the data are now provided in NetCDF format, with daily files for each underlying motion field, e.g. SSMI, buoy and wind-driven motions – as well as files containing the daily combined (optimally interpolated) estimate and a weekly average sea ice motion. The self-describing file format provides improved metadata (including georeference information) and easier access for many users. Because the passive microwave daily ice motions are at a coarse resolution, they tend to exhibit discretization effects at daily timescales. These effects are diminished when averaged over a week. Thus, the weekly sea ice motion fields are the recommended product for examining trends in sea ice velocity. The NSIDC archive also provides browse imagery of the weekly sea ice motions (Figure 5), which has also been updated to improve visual appearance.

3 The EASE-Grid Sea Ice Age Product

The EASE-Grid Sea Ice Age product [Tschudi *et al.*, 2016c] builds upon the motion product and is also a popular dataset with over 650 unique users having accessed the data as of this writing [NSIDC, personal comm.]. Version 2 of the sea ice age data is also part of NASA's Making Earth System Data Records for Use in Research (MEaSURES) dataset at NSIDC [Anderson *et al.*, 2014]; however, the MEaSURES product is not regularly updated and does not include the newest enhancements described here. Animations of motion and age have been posted on NOAA's ClimateWatch online magazine [2016] (<http://www.climate.gov/news-features/videos/old-ice-arctic-vanishingly-rare>), which had over 300 hits the first day of posting, as well as the NASA Scientific Visualization Studio (<https://svs.gsfc.nasa.gov/4509>). Sea ice age distributions and trends are described annually in the Arctic Report Card [Perovich *et al.*, 2018] and have been analyzed by Maslanik *et al.* [2007; 2011].

The Sea Ice Age product was introduced by Fowler *et al.* [2004] and described further by Maslanik *et al.* [2007; 2011], Tschudi *et al.* [2010], and Stroeve *et al.* [2011]. The ice age product algorithm estimates, in years, the age of Arctic sea ice using input from the previously described sea ice motion product. Weekly averaged motions are used to reduce computational complexity and to temporally average discretization artifacts in the daily motion data. Also, the 25 km resolution motions are bilinearly interpolated to a 12.5 km resolution grid in order to provide finer granularity in the ice age fields.

At the beginning of the ice motion record, all parcels in the 12.5 km ice age grid are initialized with an age-class of “first-year ice”, meaning ice that is less than 1 year old. These parcels are then treated as Lagrangian particles and are advected at weekly time steps with the motion product estimates. Rarely, ice motion results in all parcels being advected out of a grid cell; when this occurs, a new parcel of “first-year ice” is initialized in that grid cell. During the week of the Arctic sea ice extent minimum, the age of all parcels is incremented by one year. At each time step, all parcels found within a grid cell that has an ice concentration of less than 15% are considered to have melted and are no longer considered in determining the ice age. Parcels are tracked for up to 16 years, after which they are no longer considered.



This approach does not consider new ice that may form within a grid cell because it retains only the oldest ice in its accounting. Thus, the product is effectively an estimate of the oldest ice in a given grid cell. Tracking of partial concentration of age categories can provide a more detailed picture of the ice cover [Korosov *et al.*, 2018] and is something we may consider for future versions.

The source motion data for the age product begin in 1978. However, because the method tracks age over time, several years are needed to “spin up” to obtain the older ice categories. For this reason, the ice age product begins in 1984. The youngest ice age category is first-year ice (FYI), which is ice that is less than a year old. Similarly, second-year ice is one to two years old, and so on for older ice age categories. Ice older than 4 years (5th-year ice) makes up a very small percentage of the ice cover, so depicting ice older than this category as a separate field in browse imagery is not undertaken. Therefore, the ice age is frequently categorized as being of ages: 0-1 (i.e., FYI), 1-2, 2-3, 3-4, and more than 4 years old (i.e., 5th-year ice).

Version 4 changes. The primary changes in Version 4 of the ice age product result from the changes in the source ice motion products described above. The most substantial change addressed anomalous behavior in the motion and age fields documented by Szanyi *et al.* [2016]. They showed that discontinuities in the interpolated motion field, caused by sub-optimal interpolation of buoys with the other data sources, created artificial ice divergence and new ice formation in the Version 3 product. This potentially results in an underestimation of multi-year and an overestimation of first-year ice. The change in the interpolation weighting, described above, substantially reduced this effect. As a result, there is less “speckling” of first-year ice interspersed within the multi-year ice pack and the age fields show a more realistic consolidated multi-year ice pack. The net effect is a reduced amount of first-year ice and an increased amount of multi-year in Version 4 compared to Version 3 (Figure 6). This effect becomes much less noticeable during the latter part of the record. There are three reasons for this. First, there is less passive microwave coverage during the early SMMR period, so a sparser number of vectors, which will accentuate interpolation-induced artifacts in the data. Similarly, in the early part of the record, there were far fewer buoys, so the buoy interpolation discontinuities are more noticeable. In recent years, there are enough buoys such that the interpolation distances of neighboring buoys often overlap, so discontinuities with the passive microwave and wind fields are less common. Finally, there is simply much less multi-year ice in recent years, so the discontinuity effects are less frequent.

Two other minor changes to the ice age product have been introduced in Version 4. First, the week-numbering convention was slightly modified to be consistent with the motion weeks. Second, browse imagery (Figure 6) was improved to explicitly show ice-covered ocean areas that are outside of the age and motion domain (e.g., the Canadian Archipelago).



4 Trends and variability in Version 4 ice motion and age and comparison to Version 3

Here we evaluate how the changes from Version 3 to Version 4 of the products affect the long-term trends and variability in the sea ice age fields. We also provide updated motion age trends through 2017.

5 As seen in Figure 3, the change to Version 4 does noticeably affect parts of the daily fields in regions around buoys. Over a weekly period, the changes are less significant because the motions are smoothed out. The weekly average speed in the Arctic is generally ~ 0.5 cm/s (10-20%) faster in Version 4 and the difference with Version 3 is fairly consistent over time (Figure 7). The differences in the u and v motion components (not shown) are likewise small and consistent over the time series. There is seasonal variation with larger differences during summer. This corresponds to overall faster speeds, as seen in the Version 4
10 weekly average speed timeseries (Figure 8) that show strong seasonal variability with speeds peaking during summer. There is also interannual variability, but overall there is an increasing trend in Arctic sea ice speed of 0.21 cm/s/decade in Version 4 versus 0.13 cm/s/decade in Version 3. The increasing speed is in general agreement with previous studies that noted a trend toward faster moving ice [e.g., *Spreen et al.*, 2011] and linked the trend to greater response to wind-forcing by a thinner ice cover.

15

The largest effect of the version change for ice age is, as noted above, the amount of multi-year ice in the early part of the record, particularly in the oldest ice categories. This is illustrated in the timeseries of ice age (Figure 9). Both versions show a strong decline in 4+ year old ice over the record, with a steep loss of old ice in the late 1980s through the mid-1990s, which is associated with a persistent positive mode of the Arctic Oscillation (AO) [*Rigor et al.*, 2002]. A positive AO results in increased
20 drift from the Siberian coast and greater advection of ice out of the Arctic through Fram Strait, which serves to “drain” older ice out of the Arctic [*Rigor and Wallace*, 2004].

The change to Version 4 results in higher extent of the old ice in the early part of the record, which is an effect of the improved interpolation weighting scheme. However, the impact dissipates over time, likely due to two factors: (1) the transition from
25 SMMR to SSMI-SSMIS and the resulting improved coverage; and (2) the increasing number of buoys over time. By 2005, there is very little difference between the two versions. Focusing on the week of 19-25 February, the larger differences between versions of 4+ year old ice compared to younger ice types is evident (Figure 10). The younger ice categories show smaller, generally negative differences (i.e., less younger ice in Version 4). Thus, the changes in Version 4 appear to improve the ice age fields by removing much of the artificial divergence noted in *Szanyi et al.* [2016], thereby reducing the amount of younger
30 ice and increasing the amount of older ice. However, the impact of the version change decreases over time such that there little impact on the age distribution in recent years.



Both versions of the ice age field show a transition from one dominated by older ice to one dominated by younger ice (Figure 11). Interannual variability is evident in all ice age classes, particularly first-year ice, which is not surprising given the variability of the summer ice cover. Less variability is seen in older ice. Nonetheless, the decline in old ice is apparent during the late-1980s through the mid-1990s persistent positive mode of the Arctic Oscillation [Rigor *et al.*, 2002]. After 1994, there was some recovery in multi-year ice before beginning a significant decline after 2004. Linear trends are estimated for the Arctic Ocean region. This is a region bounded by the northern coasts of the continents, the Bering Strait, Fram Strait, and the ~20 E meridian between Svalbard and the Fennoscandian peninsula. The total area of the region is $\sim 7.8 \times 10^6$ km². Using this region excises areas where only first-year ice exists, so it focuses on the areas where there is variability in the ice age. There is a strong increasing trend in ice less than 1 year old (Table 2) and a similar decreasing trend in 4+ year old ice. Trends in the intermediate ages (1-4 years old) are smaller. This is partly due to smaller extents of these ages as well as the fact that ice transitions through these categories between the larger extents of the oldest and youngest ice.

5 Conclusions

New versions (4.0) of the sea ice motion [Tschudi *et al.*, 2016b] and sea ice age [Tschudi *et al.*, 2016c] datasets have been produced and will soon be available at NSIDC. Routine updates will regularly occur when the underlying data – buoy positions, brightness temperature fields and sea ice concentration fields – become available. This is expected to occur every few months.

Arctic sea ice motion vectors are currently constructed by merging motion vectors estimated using three sources: buoys, passive microwave satellite imagery, and winds. In the Antarctic, only the satellite imagery vectors are used. Sea ice age is produced using the weekly northern hemisphere sea ice motion product as input, tracking ice parcels and aging them each year if they neither melt nor advect out of the ice pack.

The most recent sea ice motion algorithm revision incorporates improvements such as an improved vector weighting scheme, corrections to passive microwave vectors, new browse imagery, and the underlying code base through the use of Python. Furthermore, the Version 4.0 upgrade addresses artifacts in the ice motion resulting from the interpolation, though these artifacts did not substantially affect the weekly sea ice motion or age fields.

We note the decrease in older sea ice over the ice age record, from the 1980's, when older ice constituted ~30% of the ice pack, to recent years, when older ice occupies less than 5% of the pack. Tschudi *et al.* [2016a] compared ice age to ice thickness derived from ICESat [Kwok *et al.*, 2009; Kwok and Cunningham, 2008] and NASA's IceBridge campaign [Kurtz *et al.*, 2012, 2013]. They found that the thickness/age relationship has an approximate linear fit for the ICESat dataset, but that the relationship was much more variable for IceBridge, due to the Arctic basin-wide coverage of ICESat thickness data and the more limited areal coverage for IceBridge aircraft-acquired data. The relationship found between ice age and thickness for the



basin-wide ICESat dataset suggests that the ice age product may be used as a general indication of the sea ice thickness distribution, and could be compared to other Arctic basin-wide sea ice thickness estimations, such as those from CryoSat-2 [ESA CPOM, 2015].

- 5 The ice age motion and age products are continuously being improved. We plan to utilize passive microwave imagery from the AMSR2 instrument aboard the GCOM-1 satellite in a future release of the motion product, which may reduce the error in motion, due to the improved higher spatial resolution of AMSR2 over SSMIS. We also plan to further improve the age product by categorizing the age distribution in each EASE grid cell, instead of retaining only the oldest ice age. Numerous other improvements in the sea ice motion and age products are also planned, pending support.

10

6 Acknowledgments

The authors thank the anonymous reviewers for their helpful reviews of this manuscript. Research for this manuscript is supported by the NASA Cryospheric Sciences Program, per award NNX16AQ41G, and NASA Snow and Ice Distributed Active Archive Center (DAAC) at NSIDC.

15 References

- Anderson, M. R., Bliss, A. C., and Tschudi, M.: MEASUREs Arctic Sea Ice Characterization 25 km EASE-Grid 2.0. Boulder, Colorado USA: NASA DAAC at the National Snow and Ice Data Center. doi:10.5067/MEASURES/CRYOSPHERE/nsidc-0532.001, 2014.
- Brodzik, M. J. and Knowles, K. W.: EASE-Grid: A Versatile Set of Equal-Area Projections and Grids in M. Goodchild (Ed.) Discrete Global Grids. Santa Barbara, California USA: National Center for Geographic Information & Analysis, 2002.
- 20 Cavalieri, D. J., Parkinson, C. L., Gloersen, P. and Zwally, H. J.: Sea Ice Concentrations from Nimbus-7 SMMR and DMSP SSM/I-SSMIS Passive Microwave Data, Version 1. Boulder, Colorado USA. NASA National Snow and Ice Data Center Distributed Active Archive Center. doi: <http://dx.doi.org/10.5067/8GQ8LZQVL0VL>, 1996, updated yearly.
- Comiso, J. C., Meier, W. N., and Gersten, R.: Variability and trends in the Arctic sea ice cover: Results from different techniques, *J. Geophys. Res.*, 122, 6883-6900, doi:10.1002/2017JC012768, 2017a.
- 25 Comiso, J. C., Gersten, R. A., Stock, L. V., Turner, J., Perez, G. J. and Cho, K.: Positive trend in the Antarctic sea ice cover and associated changes in surface temperature, *J. Climate*, 30, 2251-2267, doi: 10.1175/JCLI-D-16-0408.1, 2017b.
- Comiso, J.C.: Large Decadal Decline of the Arctic Multiyear Ice Cover. *J. Climate*, 25, 1176–1193. doi: 10.1175/JCLI-D-11-00113.1, 2012.



- Comiso, J. C., Parkinson, C. L., Gersten, R. and Stock, L.: Accelerated decline in the Arctic sea ice cover, *Geophys. Res. Lett.*, 35, L01703, doi:10.1029/2007GL031972, 2008.
- Emery, W. J., Fowler, C. W., Hawkins, J. and Preller, R. H.: Fram Strait satellite image derived ice motions. *J. Geophys. Res.*, 96, 4751–4768, doi: 10.1029/90JC02273, 1991.
- 5 Emery, W. J., Fowler, C. and Maslanik, J: Satellite remote sensing of ice motion, in *Oceanographic Applications of Remote Sensing*, ed. Motoyoshi Ikeda and Frederic W. Dobson. CRC Press, Boca Raton, FL, 1995.
- ESA CPOM: European Space Agency, Centre for Polar Observation and Modeling Data Portal. Available online at <http://www.cpom.ucl.ac.uk/csopr/seaice.html>, 2015.
- Fowler, C. F., Emery, W. J. and Maslanik, J. A.: Satellite-derived evolution of Arctic sea ice age: October 1978 to March 10 2003. *IEEE Geo. Rem. Sens. Lett.*, doi: 10.1109/LGRS.2004.824741, 2004.
- Francis, J. A., and Vavrus, S. J.: Evidence linking Arctic amplification to extreme weather in mid-latitudes, *Geophys. Res. Lett.*, 39, L06801, doi:10.1029/2012GL051000, 2012.
- Francis, J. A., Hunter, E., Key, J. R. and Wang, X.: Clues to variability in Arctic minimum sea ice extent. *Geophys. Res. Lett.*, 32, L21501, doi:10.129/2005GL024376, 2005.
- 15 Francis, J. A., and E. Hunter, E: Clues to changes in Arctic summer-minimum sea ice extent. 14th Conference on Satellite Meteorology and Oceanography, Atlanta, GA, 28 January – 2 February, 2006, doi: 10.1029/2005GL024376, 2006.
- Huntington, H.P., Hamilton, L.C., Brunner, R., Lynch, A., Nicolson, C., Ogilvie, A.E.J. and Voinov, A.: Toward understanding the human dimensions of the rapidly changing arctic system: insights and approaches from five HARC projects, *Reg. Environ. Change*, 7:173-186, doi:10.1007/s10113-007-0038-0, 2007.
- 20 Gloersen, P.: Nimbus-7 SMMR Polar Gridded Radiances and Sea Ice Concentrations, Version 1. Boulder, Colorado USA. NASA National Snow and Ice Data Center Distributed Active Archive Center. doi: 10.5067/QOZIVYV3V9JP, 2006.
- IABP. International Arctic Buoy Programme: updated periodically. Online at <http://iabp.apl.washington.edu/index.html>.
- Johannessen, O.M., E.V. Shalina, and W.M. Miles, 1999: Satellite evidence for an Arctic sea ice cover in transformation. *Science*, 286, 1937-1939, doi: 10.1126/science.286.5446.1937, 2008.
- 25 Kalnay, E., Kanamitsu, M., Kistler, R., Collins, W., Deaven, D., Gandin, L., Iredell, M., Saha, S., White, G., Woollen, J. and Zhu, Y.: The NCEP/NCAR 40-year reanalysis project. *Bull. Amer. Meteorol. Soc.*, 77(3), pp.437-471, doi: 10.1175/1520-0477(1996)077<0437:TNYRP>2.0.CO;2, 1996.
- Korosov, A. A., Rampal, P., Pedersen, L. T., Saldo, R., Ye, Y., Heygster, G., Lavergne, T., Aaboe, S., and Girard-Arduin, F.: A new tracking algorithm for sea ice age distribution estimation, *The Cryosphere*, 12, 2073-2085, doi:10.5194/tc-12-30 2073-2018, 2018.
- Kurtz, N., Studinger, M., Harbeck, J., Onana, V. and Farrell, S.: IceBridge Sea Ice Freeboard, Snow Depth, and Thickness, Version 1. Boulder, Colorado USA: NASA DAAC at the National Snow and Ice Data Center, doi: 10.5067/7XJ9HRV50O57, 2012, updated 2015.



- Kurtz, N. T., Farrell, S. L., Studinger, M., Galin, N., Harbeck, J. P., Lindsay, R., Onana, V. D., Panzer, B., and Sonntag, J. G.: Sea ice thickness, freeboard, and snow depth products from Operation IceBridge airborne data, *The Cryosphere*, 7, 1035-1056, <https://doi.org/doi:10.5194/tc-7-1035-2013>, 2013.
- Kurtz, N. T., Galin, N. and Studinger, M.: An improved CryoSat-2 sea ice freeboard retrieval algorithm through the use of waveform fitting, *The Cryosphere*, 8, 1217-1237, doi:10.519/tc-8-1217-2014, 2014.
- 5 Kwok, R., Schweiger, A., Rothrock, D. A., Pang, S. and Kottmeier, C.: Sea ice motion from satellite passive microwave imagery assessed with ERS SAR and buoy motions. *J. Geophys. Res.*, 103 (C4), 8,191-8,214, doi: 10.1029/97JC03334, 1998.
- Kwok, R.: Summer sea ice motion from the 18 GHz channel of AMSR-E and the exchange of sea ice between the Pacific and Atlantic sectors, *Geophys. Res. Lett.*, 35, L03504, doi:10.1029/2007GL032692, 2008.
- 10 Kwok, R., and Cunningham, G. F.: ICESat over Arctic sea ice: Estimation of snow depth and ice thickness, *J. Geophys. Res.*, 113, C08010, doi:10.1029/2008JC004753, 2008.
- Kwok, R., Cunningham, G. F., Wensnahan, M., Rigor, I., Zwally, H.J. and Yi, D.: Thinning and volume loss of the Arctic Ocean sea ice cover: 2003–2008, *J. Geophys. Res.*, 114, C07005, doi:10.1029/2009JC005312, 2009.
- 15 Kwok, R.: Arctic sea ice thickness, volume, and multiyear ice coverage: losses and coupled variability (1958-2018), *Env. Res. Letters*, 13, 105005, doi:10.1088/1748-9326/aae3ec, 2018.
- Laxon, S. et al.: CryoSat-2 estimates of Arctic sea ice thickness and volume, *Geophys. Res. Lett.*, 40, 1-6, doi:10.1002/GRL.50193, 2013.
- Lynch, A. H., Curry, J. A., Brunner, R. D., and Maslanik, J. A.: Towards an integrated assessment of the impacts of extreme wind events on Barrow, Alaska. *Bull. Amer. Meteorol. Soc.*, 85, 209–221, doi: 10.1175/BAMS-85-2-209, 2004.
- 20 Markus, T., and several co-authors: The Ice, Cloud, and land Elevation Satellite-2 (ICESat-2): Science requirements, concept, and implementation, *Rem. Sens. Environ.*, 190, 260-273, doi:10.1016/j.res.2016.12.029, 2017.
- Maslanik, J., Stroeve, J., Fowler, C. and Emery, W.: Distribution and trends in Arctic sea ice age through spring 2011. *Geophys. Res. Lett.*, 38, L13502, doi:10.1029/2011GL047735, 2011.
- 25 Maslanik, J.A., Fowler, C., Stroeve, J., Drobot, S., Zwally, J., Yi, D. and Emery, W.: A younger, thinner Arctic ice cover: Increased potential for rapid, extensive sea-ice loss, *Geophys. Res. Lett.*, 34, L24501, doi:10.1029/2007GL032043, 2007.
- Maslanik, J. and Stroeve, J.: *DMSP SSM/I-SSMIS Daily Polar Gridded Brightness Temperatures, Version 4*. Boulder, Colorado USA. NASA National Snow and Ice Data Center Distributed Active Archive Center. <https://doi.org/10.5067/AN9AI8EO7PX0>, 2004.
- 30 Maslanik, J. and Stroeve, J.: *Near-Real-Time DMSP SSMIS Daily Polar Gridded Sea Ice Concentrations, Version 1*. Boulder, Colorado USA. NASA National Snow and Ice Data Center Distributed Active Archive Center. <https://doi.org/10.5067/U8C09DWVX9LM>, 1999, updated daily.
- Meier, W. N., Maslanik, J. A. and Fowler, C. W.: Error analysis and assimilation of remotely sensed ice motion within an Arctic sea ice model, *J. Geophys. Res.*, 105(C2), 3339–3356, doi:10.1029/1999JC900268, 2000.



- Meier, W.N. and Dai, M.: High-resolution sea-ice motions from AMSR-E imagery, *Ann. Glaciol.*, 44, 352-356, doi: 10.3189/172756406781811286, 2006.
- Meier, W. N., et al.: Arctic sea ice in transformation: A review of recent observed changes and impacts on biology and human activity, *Rev. Geophys.*, 51, 185–217, doi:10.1002/2013RG000431, 2014.
- 5 NOAA's Climate Watch: Available online at <http://www.climate.gov/news-features/videos/old-ice-arctic-vanishingly-rare>, 2016.
- Overland, J. E.: A difficult Arctic science issue: Midlatitude weather linkages, *Polar Science*, 10, 210-216, doi:10.1016/j.polar.2016.04.011, 2016.
- Parkinson, C. L., & Cavalieri, D. J.: Antarctic sea ice variability and trends, 1979-2010. *The Cryosphere*, 6, 871–880, doi: 10.5194/tc-6-871-2012, 2012.
- 10 Perovich, D., Meier, W., Tschudi, M., Farrell, S., Hendricks, S., Gerland, S., Haas, C., Krumpfen, T., Polashenski, C., Ricker, R., Webster, M.: *Sea Ice* in [Arctic Report Card 2018], <https://www.arctic.noaa.gov/Report-Card>, 2018.
- Pizzolato, L., Howell, S. E. L., Dawson, J., Laliberté, F. and Copland, L.: The influence of declining sea ice on shipping activity in the Canadian Arctic, *Geophys. Res. Lett.*, 43, doi:10.1002/2016GL071489, 2016.
- 15 Rigor, I.G., Wallace, J. M. and Colony, R. L.: Response of sea ice to the Arctic Oscillation, *J. Climate*, 15, 2648-2663, doi:10.1175/1520-0442(2002)015<2648:ROSITT>2.0.CO;2, 2002.
- Rigor, I.G., and Wallace, J. M.: Variations in the age of Arctic sea-ice and summer sea-ice extent, *Geophys. Res. Lett.*, 31, L09401, doi:10.1029/2004GL019492, 2004.
- Sewall, J.: Precipitation Shifts over Western North America as a Result of Declining Arctic Sea Ice Cover: The Coupled System Response. *Earth Interactions*, Vol. 9, No. 26, doi:10.1175/EI171.1, 2005.
- 20 Spreen, G., Kwok, R. and D. Menemenlis, D.: Trends in Arctic sea ice drift and role of wind forcing: 1992-2009, *Geophys. Res. Lett.*, 38, L19501, doi:10.1029/2011GL048970, 2011.
- Stroeve, J., Barrett, A., Serreze, M. and Schweiger, A.: Using records from submarine, aircraft and satellites to evaluate climate model simulations of Arctic sea ice thickness, *The Cryosphere*, 8(5), 1839-1854, doi:10.5194/tc-8-1839-2014, 2014.
- 25 Stroeve, J. C., Serreze, M. C., Kay, J. E., Holland, M. M., Meier, W. N. and Barrett, A. P.: The Arctic's rapidly shrinking sea ice cover: A research synthesis, *Climatic Change*, doi:10.1007/s10584-011-1010-1, 2011.
- Sumata, H., Lavergne, T., Girard-Ardhuin, F., Kimura, N., Tschudi, M. A., Kauker, F., Karcher, M. and Gerdes, R.: An intercomparison of Arctic ice drift products to deduce uncertainty estimates, *J. Geophys. Res. Oceans*, 119, 4887–4921, doi:10.1002/2013JC009724, 2014.
- 30 Szanyi, S., Lukovich, J. V., Barber, D. G., and Haller, G.: Persistent artifacts in the NSIDC ice motion data set and their implications for analysis, *Geophys. Res. Lett.*, 43, 10,800–10,807, doi:10.1002/2016GL069799, 2016.
- Thorndike, A. S., and Colony, R.: Sea ice motion in response to geostrophic winds, *J. Geophys. Res.*, 87(C8), 5845–5852, doi:10.1029/JC087iC08p05845, 1982.



- Tilling, R.L., Ridout, A. and Shepherd, A.: Near-real-time Arctic sea ice thickness and volume from CryoSat-2, *The Cryosphere*, 10, 2003–2012, doi:10.5194/tc-10-2003-2016, 2016.
- Tschudi, M.A., J.C. Stroeve, J. C. and Stewart, J. S.: Relating the Age of Arctic Sea Ice to its Thickness, as Measured during NASA's ICESat and IceBridge Campaigns. *Remote Sens.*, 8(6), 457, doi: 10.3390/rs8060457, 2016a.
- 5 Tschudi, M., Fowler, C., Maslanik, J., Stewart, J. S. and Meier, W. N.: Polar Pathfinder Daily 25 km EASE-Grid Sea Ice Motion Vectors. Version 3. Boulder, Colorado USA: National Snow and Ice Data Center. doi: <http://dx.doi.org/10.5067/O57VAIT2AYYY>, 2016b.
- Tschudi, M., Fowler, C., Maslanik, J., Stewart, J. S. and Meier, W. N.: EASE-Grid Sea Ice Age, Version 3. Boulder, Colorado USA. NASA National Snow and Ice Data Center Distributed Active Archive Center. doi:
10 <http://dx.doi.org/10.5067/PFSVFZA9Y85G>, 2016c.
- Tschudi, M.A., Fowler, C, Maslanik, J.A. and Stroeve, J.C.: Tracking the movement and changing surface characteristics of Arctic sea ice. *IEEE J. Selected Topics in Earth Obs. And Rem. Sens.*, 10.1109/JSTARS.2010.2048305, 2010.
- Uttal, T., et al.: Surface Heat Budget of the Arctic Ocean. *Bull. Amer. Meteor. Soc.*, 83, 255–275, doi: 10.1175/1520-0477(2002)083<0255:SHBOTA>2.3.CO;2, 2002.
- 15 Vermaire, J. C., Pisaric, M. F. J., Thienpont, J.R., Mustaphi, C. J., Kokelj, S. V., and Smol, J. P.: Arctic climate warming and sea ice declines lead to increased storm surge activity, *Geophys. Res. Lett.*, 40, 1386–1390, doi:10.1002/grl.50191, 2013.



Table 1: Version histories of the sea ice motion and age products.

Version	NSIDC Release Date	Motion	Age
1	Not distributed by NSIDC	Original version based on SMMR, SSMI, and AVHRR imagery, and buoy motions	Original research product
2	Sep 2013 (motion) Dec 2014 (age)	<ul style="list-style-type: none"> Added AMSR-E sources Added NCEP/NCAR wind-derived motions for Arctic 	<ul style="list-style-type: none"> First version distributed at NSIDC (as Version 2) Used Version 2 ice motion product as input
3	Feb 2016	<ul style="list-style-type: none"> Removed erroneous buoy and AVHRR-derived motions Updated buoys motions through most recent date Derived sea ice mask from NSIDC* product instead of internally derived concentration estimates Used GDAL** library to interpolate SSMI fields from polar stereographic to EASE grid Improved browse images 	<ul style="list-style-type: none"> Used Version 3 ice motion as input Improved browse images
4	Nov 2018	<ul style="list-style-type: none"> Used highest-weighted vectors for interpolated gridded fields instead of nearest vectors Daily buoy motions averaged instead of using latest observation Open water buoys removed Final quality-controlled SSMI and SSMIS brightness temperatures used throughout record Corrected over-filtering of SSMI and SSMIS vectors that had removed valid motion Improved browse images 	<ul style="list-style-type: none"> Used Version 4 ice motion input Updated week-numbering convention to be consistent with motions Improved browse images

*Cavalieri et al., 1996; **Geospatial Data Abstraction Library (<https://gdal.org>).



Table 2. Linear trends for ice ages over three periods. The main values are for Version 4, with Version 3 values in italics on the line below. These values are for the Arctic Ocean region.

Sea ice age	1984-2017 Trend [km ² /year]	1984-1996 Trend [km ² /year]	1997-2017 Trend [km ² /year]
0-1	69,200 <i>(67,700)</i>	96,200 <i>(94,000)</i>	92,500 <i>(95,600)</i>
1-2	10,500 <i>(4,900)</i>	22,100 <i>(18,000)</i>	4,500 <i>(-3,500)</i>
2-3	-4,900 <i>(-7,300)</i>	10,000 <i>(2,000)</i>	-12,500 <i>(-11,900)</i>
3-4	-10,100 <i>(-11,200)</i>	-11,400 <i>(-9,000)</i>	-16,100 <i>(-16,700)</i>
4+	-75,500 <i>(-64,800)</i>	-104,100 <i>(-91,000)</i>	-93,300 <i>(-88,000)</i>

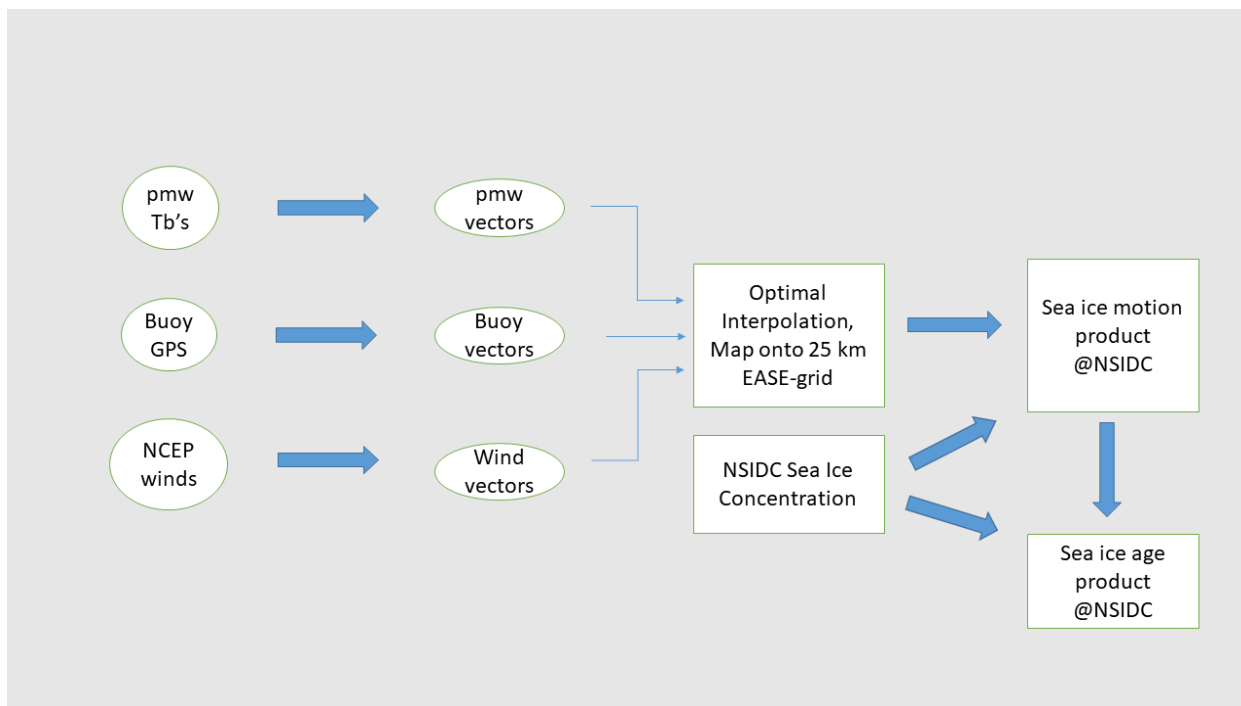


Figure 1: Flow chart for the production of the sea ice motion and age products.

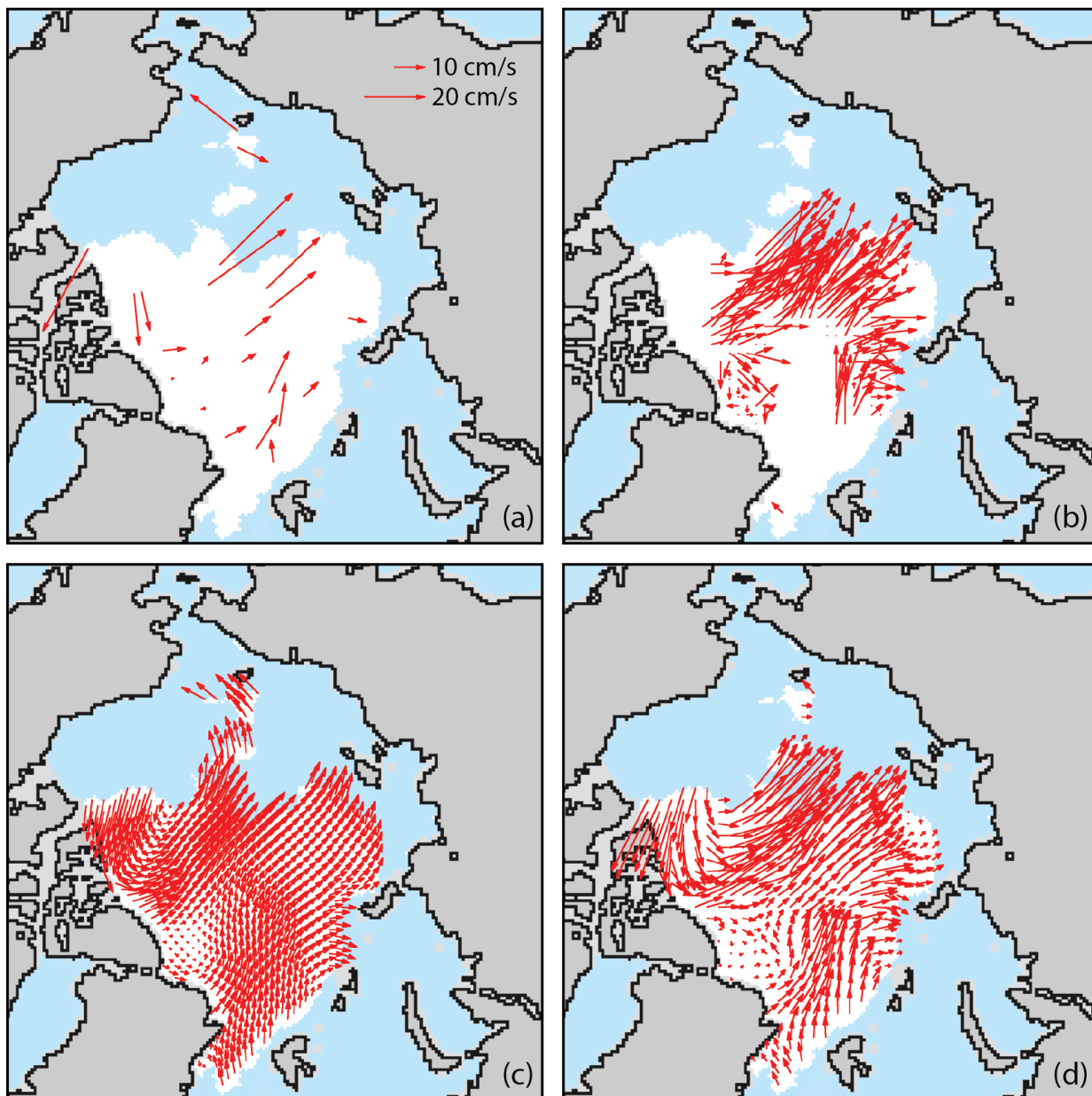
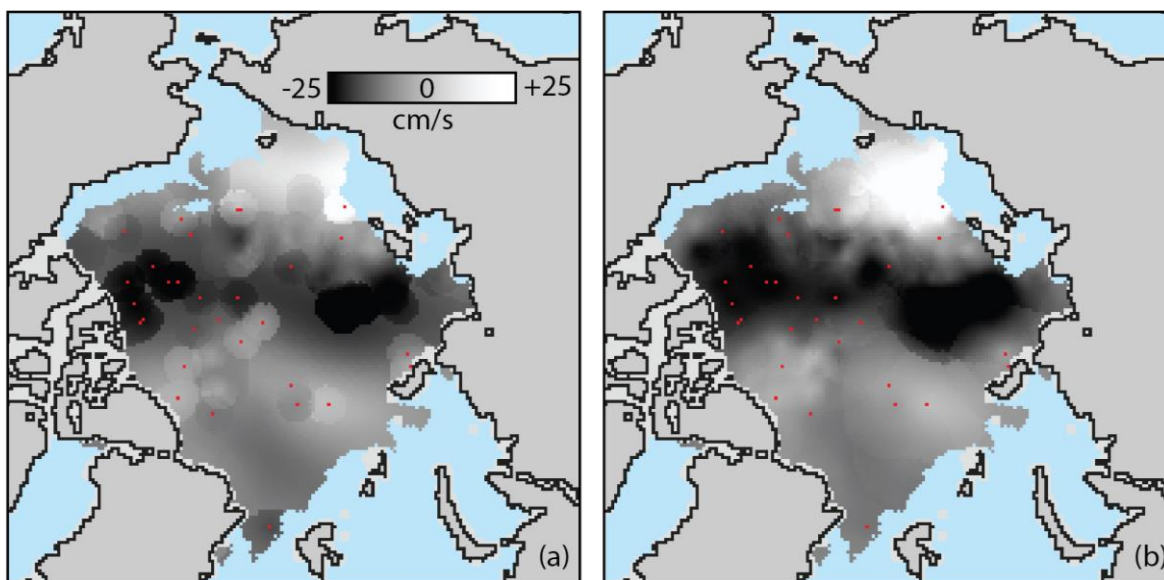
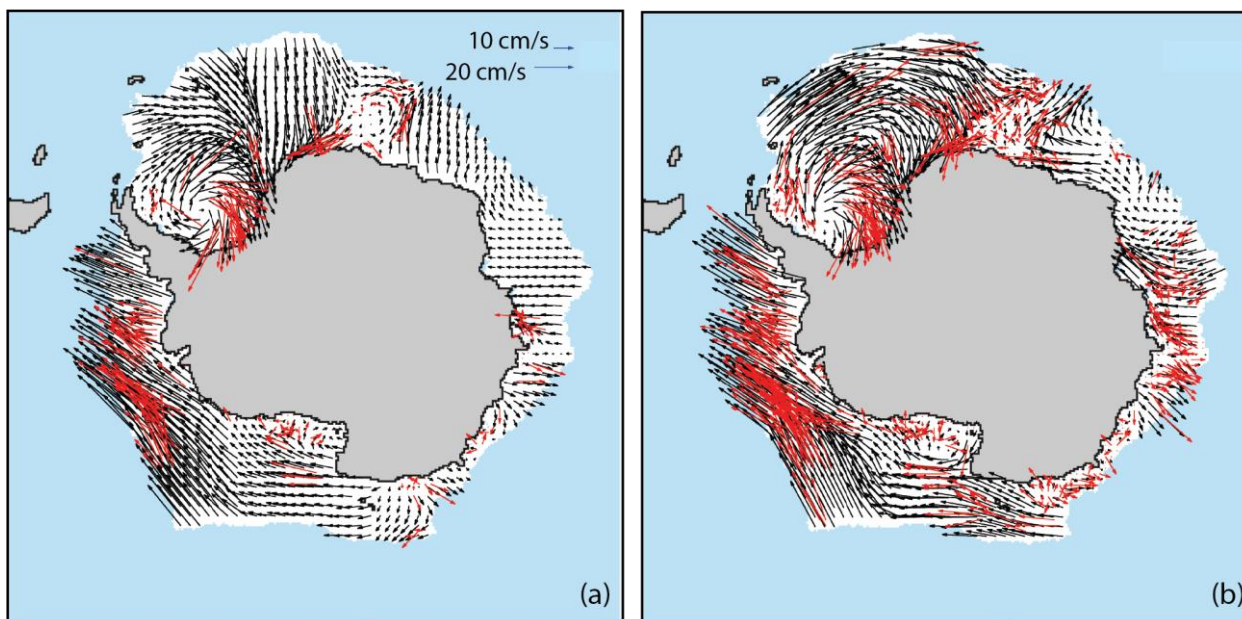


Figure 2: September 16, 2016 daily motion vectors from (a) buoys, (b) passive microwave, and (c) winds. The three sources are then merged to form (d) the daily interpolated sea ice motion field. Sea ice (white), ice-free ocean (blue), land (gray) and coast (black) are also shown. All buoys are shown, but other fields show only every 4th vector for legibility.

5



5 Figure 3: U-component of the daily interpolated vector field for September 17, 2001 from (a) Version 3 and (b) Version 4. The Version 3 fields show sharp gradients in the velocity when highly-weighted buoy estimates – buoy locations shown with red dots – no longer contribute to the motion field. Version 4 removes these sharp gradients by considering the highest weighted - rather than closest - underlying estimates.



10 Figure 4: Version 3 (a) and Version 4 (b) Antarctic SSMI vectors (red) and resulting interpolated vectors (black) for August 22, 2001. Version 3 over-filtered the number of underlying SSMI vectors, often resulting in an ice field constructed from very sparse underlying data. Version 4 corrected this and includes more SSMI vectors. Every 4th vector is plotted for easier legibility.

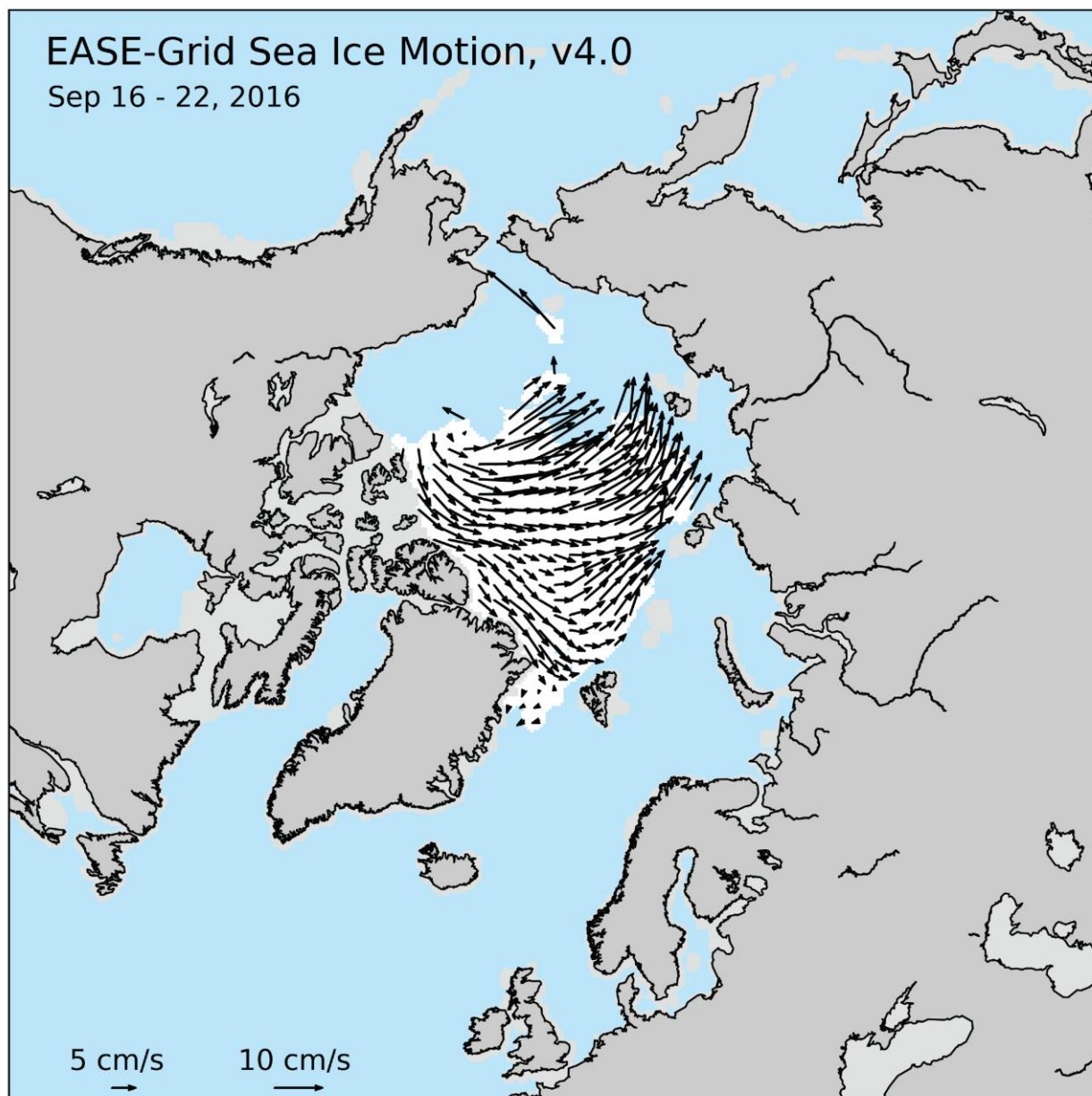


Figure 5: Example EASE-Grid sea ice motion for the Arctic region, the week of September 16-22, 2016. White indicates the sea ice mask region (>15% concentration). Note that motions are not retrieved in the Canadian Archipelago region or near coasts. Every 4th vector is plotted for easier legibility.

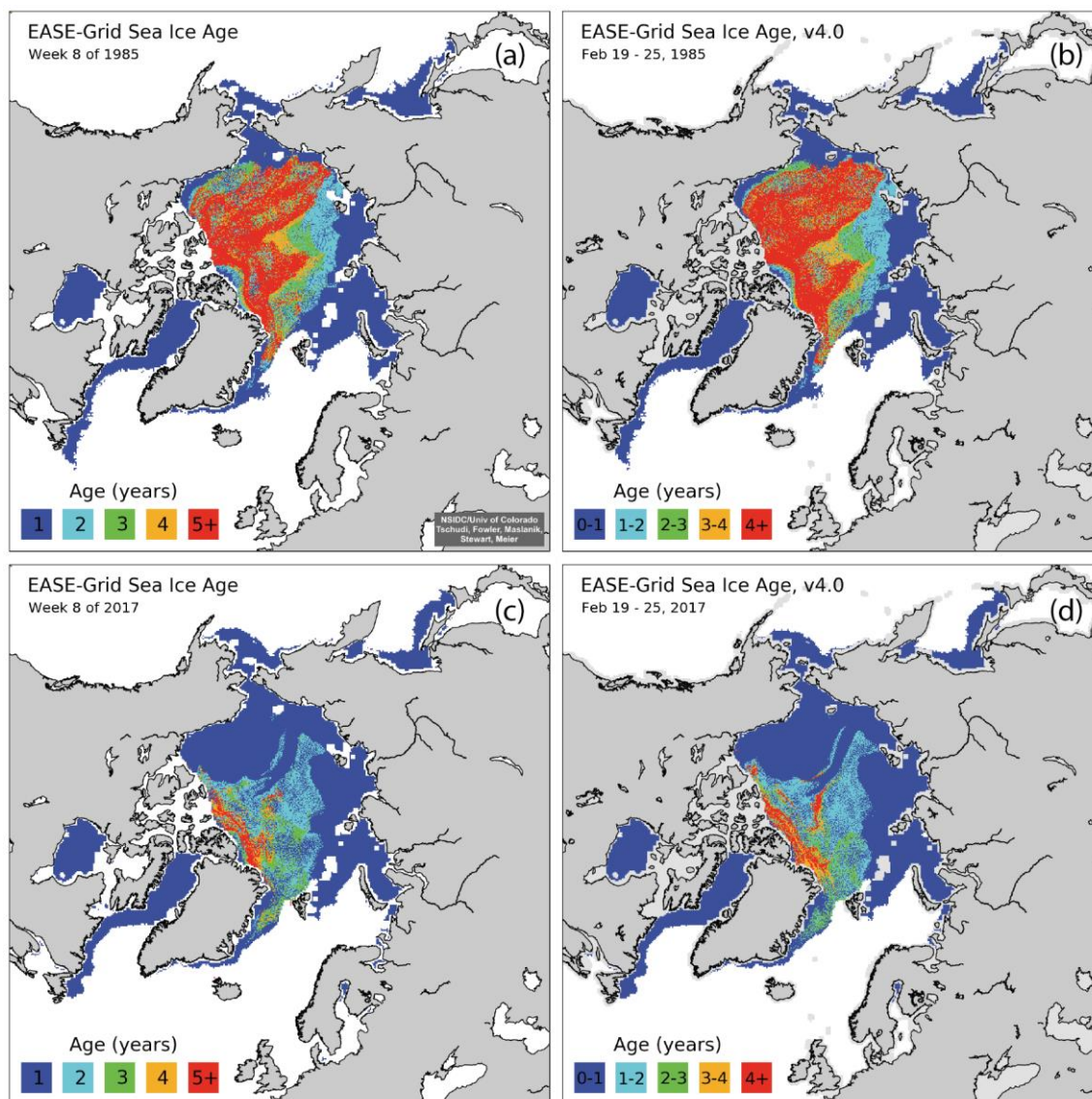


Figure 6. Comparison of Week 8 (Feb 19-25) ice ages for 1985 (a) Version 3 and (b) Version 4, and for 2017 (c) Version 3 and (d) Version 4.

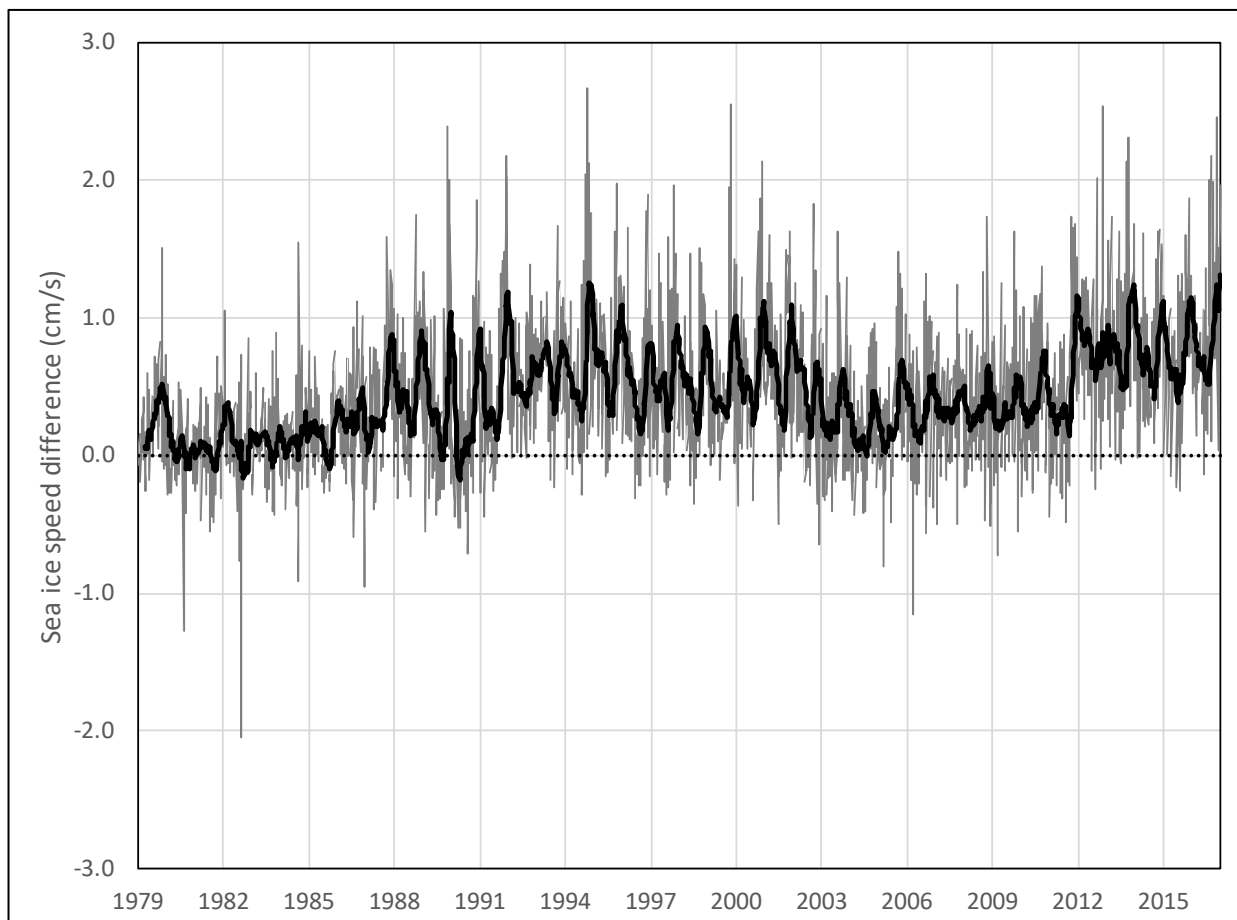


Figure 7. Arctic weekly average sea ice drift speed difference between Version 4 and Version 3 (V4-V3), 1979-2017. A 13-week running average is overlaid on the weekly values to highlight seasonal variability.

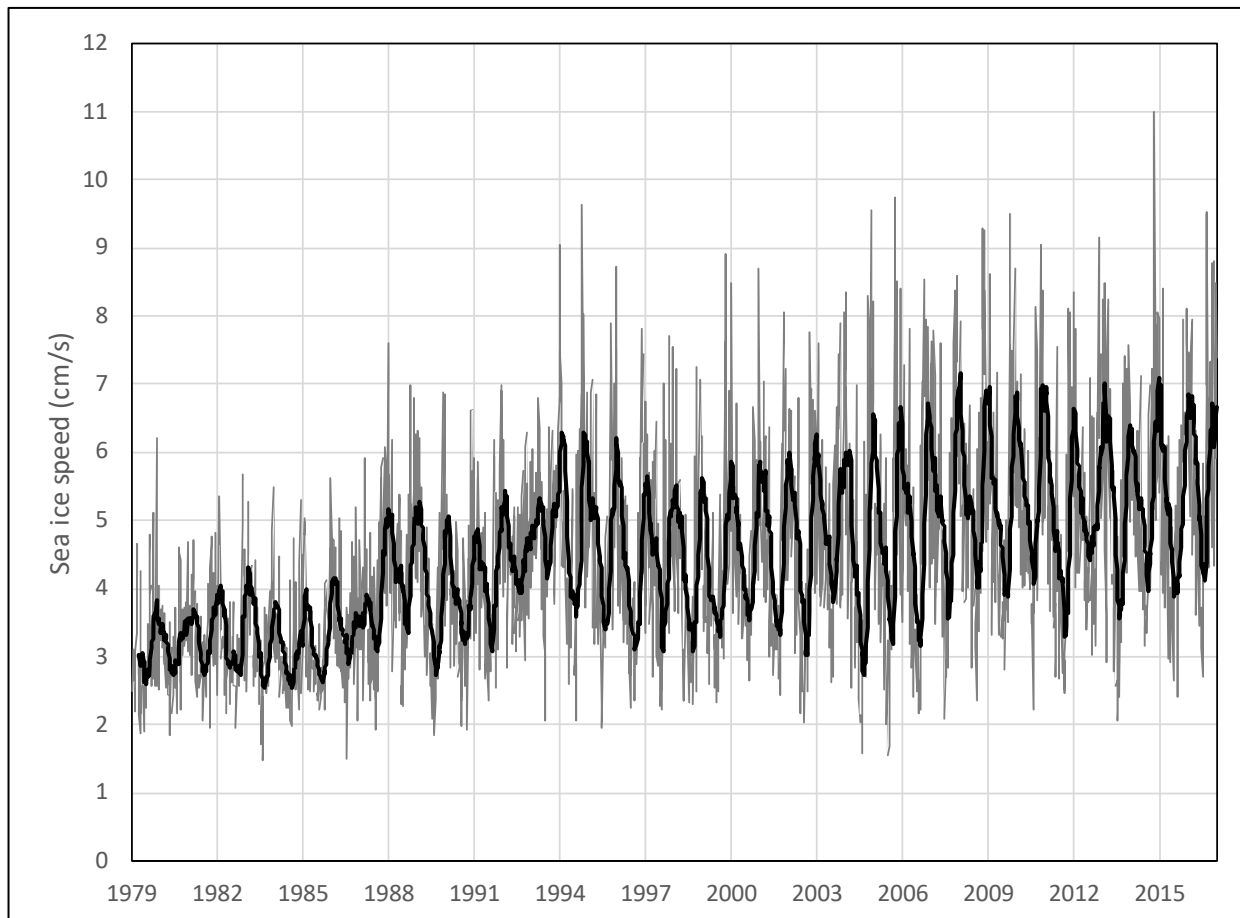


Figure 8. Arctic weekly average sea ice drift speed for Version 4, 1979-2017. A 13-week running average is overlaid on the weekly values to highlight seasonal variability.

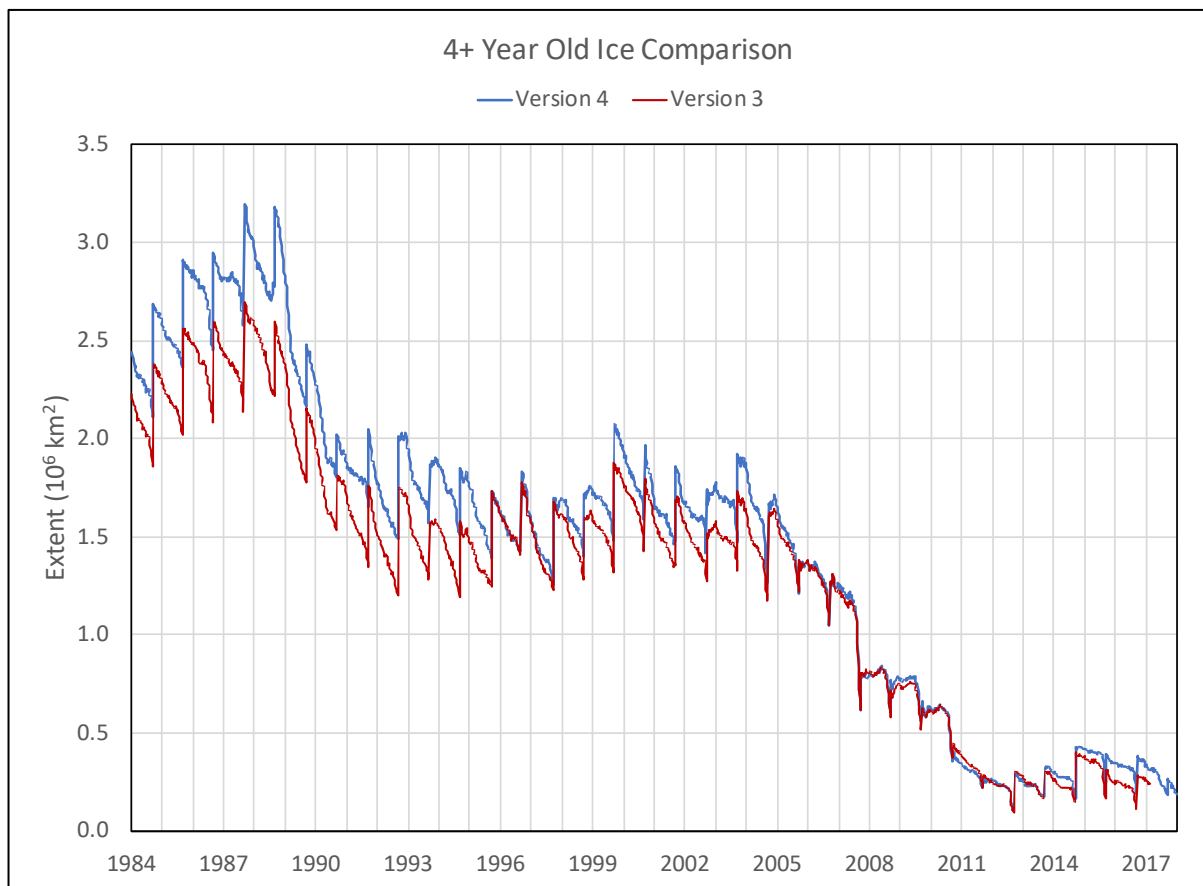


Figure 9. Comparison of 4+ year old ice from Version 3 (red) and Version 4 (blue) for 1984-2017.

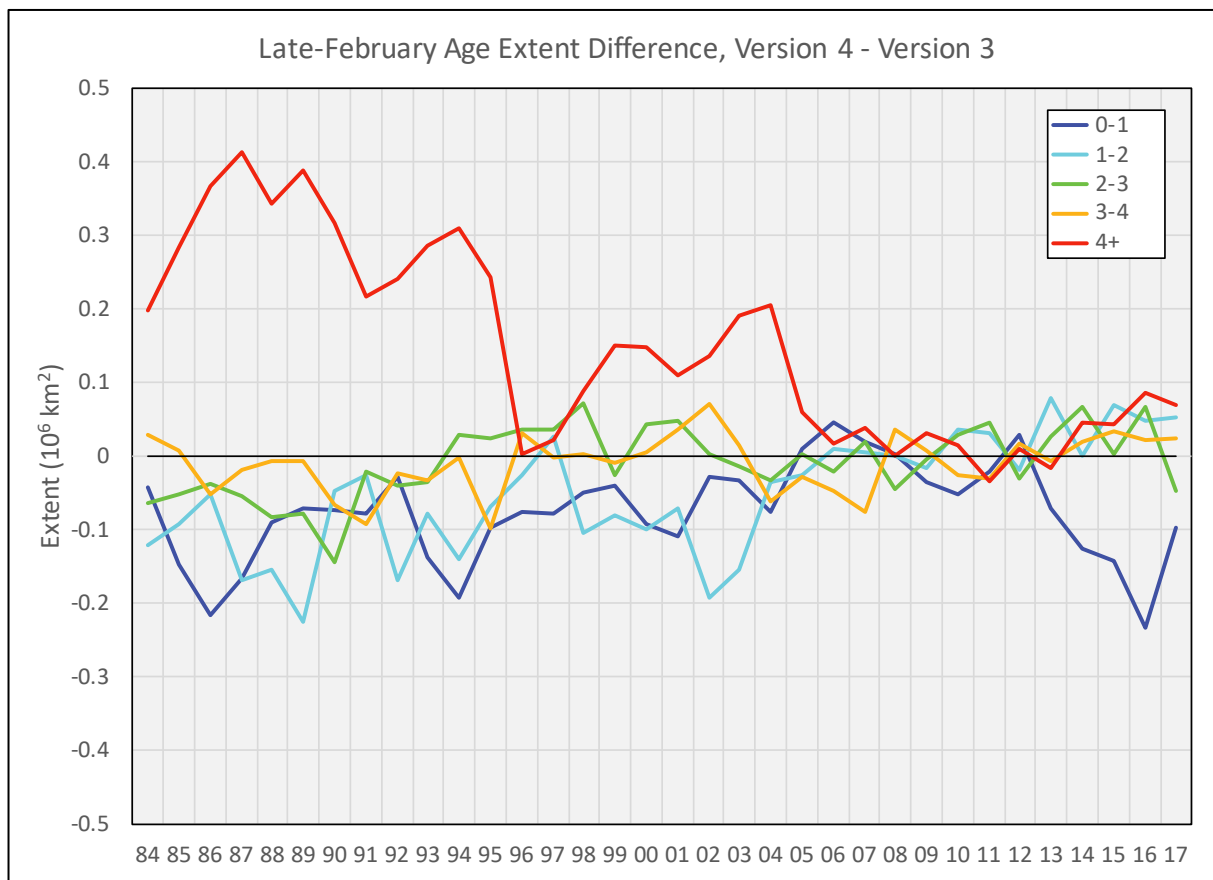


Figure 10. Extent difference between Version 4 and Version 3 sea ice age categories for the week of February 19-25 from 1984 to 2017.

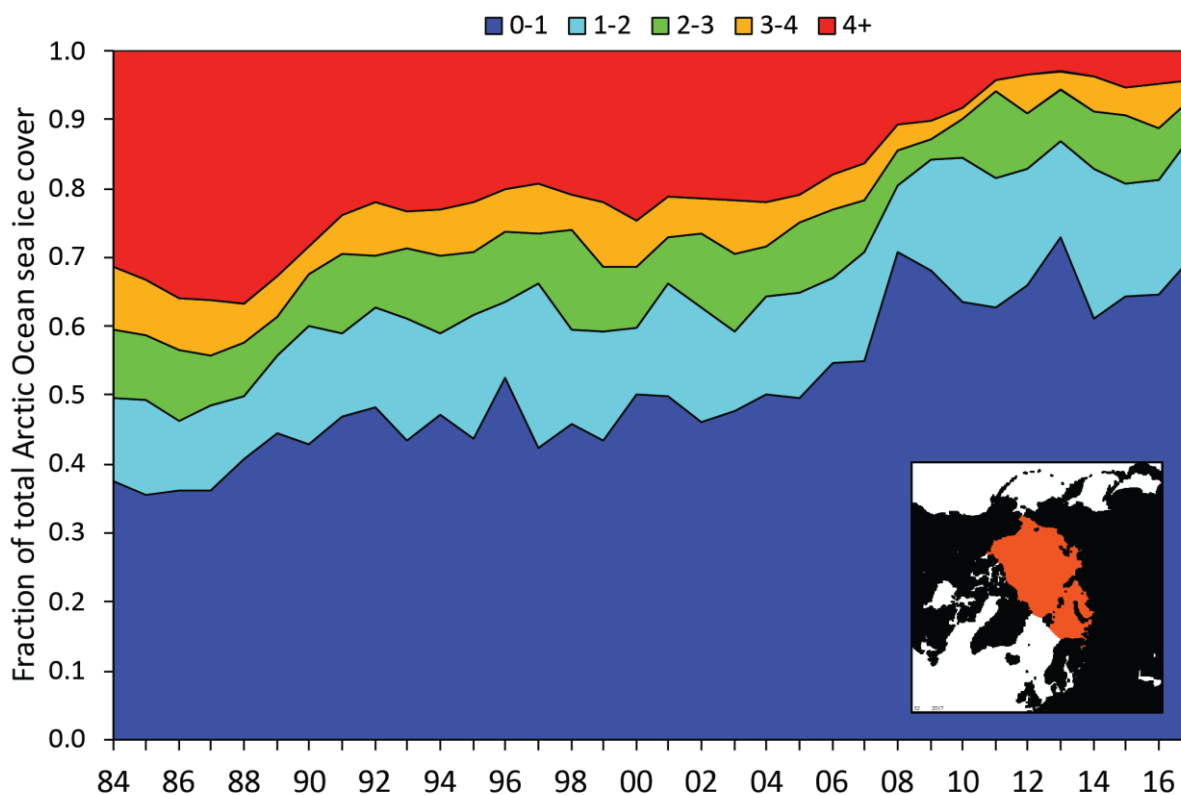


Figure 11: Trends in fraction of total sea ice coverage by sea ice age category for the week of February 19-25, 1984-2017. These trends are for the Arctic Ocean region, which is the region shaded in orange in the lower right inset image.

5

10

15